



# AFRL-RX-WP-TR-2022-0124

# LARGE - AREA FLAT LENSES FOR DRASTIC REDUCTION IN WEIGHT FOR DARPA EXTREME

**Rajesh Nenon**
**OBLATE OPTICS, INC.**

**27 JUNE 2022**
**Final Report**

**DISTRIBUTION STATEMENT A. Approved for public release;**
**Distribution is unlimited.**

**AIR FORCE RESEARCH LABORATORY**
**MATERIALS AND MANUFACTURING DIRECTORATE**
**WRIGHT-PATTERSON AIR FORCE BASE, OH 45433-7750**
**AIR FORCE MATERIEL COMMAND**
**UNITED STATES AIR FORCE**

# NOTICE AND SIGNATURE PAGE

Using Government drawings, specifications, or other data included in this document for any purpose other than Government procurement does not in any way obligate the U.S. Government. The fact that the Government formulated or supplied the drawings, specifications, or other data does not license the holder or any other person or corporation; or convey any rights or permission to manufacture, use, or sell any patented invention that may relate to them.

Qualified requestors may obtain copies of this report from the Defense Technical Information Center (DTIC) (http://www.dtic.mil).

AFRL-RX-WP-TR-2022-0124, HAS BEEN REVIEWED AND IS APPROVED FOR PUBLICATION IN ACCORDANCE WITH ASSIGNED DISTRIBUTION STATEMENT.

URBAS.AUGUSTINE.M.1267830750 Digitally signed by URBAS.AUGUSTINE.M.1267830750 Date: 2022.08.16 09:52:08 -04'00'

AUGUSTINE URBAS
Program/Project Manager/Engineer
Nanoelectronic Materials Branch
Functional Materials Division
Materials and Manufacturing Directorate

SCHMITT.MARK.G.1257789701 Digitally signed by SCHMITT.MARK.G.1257789701 Date: 2022.08.16 13:11:05 -04'00'

MARK SCHMITT
Branch Chief
Nanoelectronic Materials Branch
Functional Materials Division
Materials and Manufacturing Directorate

This report is published in the interest of scientific and technical information exchange, and its publication does not constitute the Government's approval or disapproval of its ideas or findings.

| REPORT DOCUMENTATION PAGE | Form Approved OMB No. 0704-0188 |
|---|---|



| 1. REPORT DATE *(DD-MM-YY)* | 2. REPORT TYPE | 3. DATES COVERED *(From - To)* |
|---|---|---|
| 27 June 2022 | FINAL | 20 February 2020 – 22 June 2022 |

| 4. TITLE AND SUBTITLE | 5a. CONTRACT NUMBER |
|---|---|
| LARGE AREA FLAT LENSES FOR DRASTIC REDUCTION IN WEIGHT FOR DARPA EXTREME | FA8650-20-C-7020 |
| | 5b. GRANT NUMBER |
| | 5c. PROGRAM ELEMENT NUMBER 63011F |
| 6. AUTHOR(S) Rajesh Menon | 5d. PROJECT NUMBER 1200 |
| | 5e. TASK NUMBER |
| | 5f. WORK UNIT NUMBER X1X8 |

| 7. PERFORMING ORGANIZATION NAME(S) AND ADDRESS(ES) | 8. PERFORMING ORGANIZATION REPORT NUMBER |
|---|---|
| OBLATES OPTICS, INC<br>13060 Brixton Place<br>San Diego, CA 92130 1325E | |
| 9. SPONSORING/MONITORING AGENCY NAME(S) AND ADDRESS(ES)<br>Air Force Research Laboratory<br>Materials and Manufacturing Directorate<br>Wright-Patterson Air Force Base, OH 45433-7750<br>Air Force Materiel Command<br>United States Air Force | 10. SPONSORING/MONITORING AGENCY ACRONYM(S) AFRL/RXAN<br>11. SPONSORING/MONITORING AGENCY REPORT NUMBER(S) AFRL-RX-WP-TR-2022-0124 |

12. DISTRIBUTION/AVAILABILITY STATEMENT

DISTRIBUTION STATEMENT A. Approved for public release; distribution is unlimited.

13. SUPPLEMENTARY NOTES

Report contains color. AFRL Public Affairs clearance # AFRL-2022-4178.

14. ABSTRACT

This report was developed under a DARPA contract for design, fabrication and characterization of a MWIR (3um to 5um) flat lens that can be utilized with the curved focal-plane array being developed under the DARPA FOCII program.

15. SUBJECT TERMS

Diffractive optics, mid-wave infra-red optics, grayscale lithography, inverse design.

| 16. SECURITY CLASSIFICATION OF: | | | 17. LIMITATION OF ABSTRACT: | 18. NUMBER OF PAGES | 19a. NAME OF RESPONSIBLE PERSON (Monitor) |
|---|---|---|---|---|---|
| a. REPORT Unclassified | b. ABSTRACT Unclassified | c. THIS PAGE Unclassified | SAR | 36 | Augustine Urbas<br>19b. TELEPHONE NUMBER *(Include Area Code)* (937) 255-9713 |

Standard Form 298 (Rev. 8-98)
Prescribed by ANSI Std. Z39-18

## Table of Contents

**Section** **Page**

List of Figures ..... ii

List of Tables ..... iii

1. Summary ..... 1

2. Introduction ..... 2

3. Methods, Assumptions, and Procedures ..... 13

4. Results and Discussion ..... 16

5. Conclusion ..... 25

6. References ..... 26

LIST OF SYMBOLS, ABBREVIATIONS, AND ACRONYMS ..... 29

## List of Figures

**Figure** **Page**

Figure 1:Overview of MDLs. (a) Photograph showing an MDL fabricated in a 2.3um-thick polymer film atop a 0.6mm-thick glass wafer. Optical micrographs of a portion of (b) a free-form MDL and (c) a radially-symmetric MDL. ..... 4

Figure 2: Summary of experimentally demonstrated MDLs. ..... 5

Figure 3: Summary of preliminary LWIR MDL.[3] (a) Design. (b-f): Simulated PSFs. (g) Optical micrograph and (h) Photograph of fabricated device (polymer on Si). (i) Imaging setup with microbolometer array sensor. (j) Exemplary image of a heated resistor coil. $z_o$ and $z_i$ are the object and image distances, respectively. ..... 6

Figure 4: Preliminary results from a MWIR MDL. (a) Optical micrograph of a fabricated MDL (photopolymer on silicon). (b) Image using this MDL (Courtesy of Dr. Nansheng Tang at L3Harris)..... 6

Figure 5: Imaging from the visible to the LWIR using a single MDL. The visible and NIR images were taken using the silicon CMOS image sensor. The LWIR images were taken using a FLIR Tau2 camera sensor. The remaining images used the BST microbolometer focal plane array. The MDL with glass substrate was used for visible and NIR wavelengths, while the MDL with Si substrate was used for all other wavelengths. Note that all images are raw and unprocessed. Also see corresponding videos in Supplementary Videos 1-8. Note that for the SWIR-MWIR-LWIR images, the lower wavelength cut-off arises from transmission of the silicon substrate, and no filters were used. Work performed in collaboration with Dr. Philip Hon at Northrop Grumman. ..... 7

Figure 6: The MDL has excellent aberrations performance. (a) Simulated aberrations coefficient of the LWIR MDL shown in Fig. 3. (b) Experimentally obtained aberrations coefficients for a visible-NIR MDL, also compared to a conventional refractive (stock) lens from Thorlabs. (c) Measured wavefront of this MDL under broadband visible illumination. ..... 8

Figure 7: Off-axis performance. (a) The MDL can be designed to minimize off-axis aberrations to enable large FOV. Simulated (b) PSFs and (c) focusing efficiency of one such visible MDL with FOV ~$100^0$..... 8

Figure 8: MDL with NA=0.9 (f#=0.24). (a) Optical micrograph, and 3D confocal image of (b) inner rings and (c) outer rings. (d) Measured PSF. (e) Measured MTF. ..... 9

Figure 9: Preliminary experimental results using the 2 flat lenses in tandem. (a) Schematic. (b), (c) Optical micrographs of fabricated flat lenses. (d) Color images taken with two flat lenses and the color CMOS image sensor under different illumination conditions. ..... 11

Figure 10: Schematic of MDL imaging onto a curved FPA. The radius of curvature of the FPA is exaggerated for clarity. ..... 14

Figure 11: Fabrication process. The device is created by repeated (aligned) lithography and etch steps. With N steps, one can attain 2N levels. Scanning-electron micrographs of two examples made in silicon are shown. ..... 15
Figure 12: POC (Base) design in silicon containing 5000 rings. ..... 16
Figure 13: Simulated PSFs for the flat image sensor. ..... 17
Figure 14: Simulated PSFs for a flat FPA with a larger range. ..... 18
Figure 15: Simulated aberrations (distortion and lateral chromatic aberrations) for the flat FPA. ..... 18
Figure 16: Simulated PSFs for a FPA with radius of curvature = 40mm. ..... 19
Figure 17: Simulated aberrations (distortion and lateral chromatic aberrations) for a FPA with radius of curvature = 40mm. ..... 19
Figure 18: Simulated PSFs for a FPA with radius of curvature = 24mm. ..... 20
Figure 19: Simulated aberrations (distortion and lateral chromatic aberrations) for a FPA with radius of curvature = 24mm. ..... 20
Figure 20: Simulated PSFs for a FPA with radius of curvature = 12.5mm. ..... 21
Figure 21: Simulated aberrations (distortion and lateral chromatic aberrations) for a FPA with radius of curvature = 12.5mm. ..... 21
Figure 22: Photograph of fabricated devices. ..... 22
Figure 23: Measured ring-heights from the fabricated device (top) and design (bottom). ..... 23
Figure 24: Imaging Experiments. ..... 23
Figure 25: The object was moved across the FOV of the lens to estimate its FOV as illustrated. 24

## List of Tables

**Table** **Page**

Table 1: Comparison between MDLs and metalenses. ..... 10
Table 2: Compare Oblate Flat Lens to conventional Refractive and Diffractive lenses. ..... 10
Table 3: Parameters for POC MDL. ..... 12
Table 4: Parameters of the flat lens. ..... 16

## 1. Summary

The weight of conventional refractive optics used in cameras can be too high. Multiple refractive lenses are required to correct for image aberrations (including chromatic and off-axis aberrations). Oblate Optics has developed a novel approach to replace these multi-lens imaging systems with **a single fully-aberration corrected flat lens** with no compromise in image quality. Furthermore, our lens can be up to two orders of magnitude lighter than a comparable refractive lens. Another important advantage of our technology is that when manufactured at volume, their costs can be lower as well. We have demonstrated lenses with high efficiency over very broad bandwidths and at high numerical apertures. We have also demonstrated concatenating two flat lenses for focus adjustment. In this effort, Oblate Optics performed the design, fabrication and characterization of a MWIR (3μm to 5μm) flat lens that can be utilized with the curved focal-plane array being developed under the DARPA FOCII program. One of the goals of the program is to achieve very wide field of view imaging of at least 120$^{o}$ full angle.

Specifically, during the base period we performed optimization-based design and numerical verification of a flat lens with operating wavelength in the MWIR band, f# = 2 and focal length of 20mm. Although the option period of this effort was not funded, we were also able to fabricate a prototype lens and characterize its performance.

It is recommended that follow-on efforts should include improved algorithms for the design as well as advanced semiconductor fabrication methods for the lenses.

## 2. Introduction

Using cameras in UAVs and small arms fire control is extremely useful for remote and persistent surveillance[9,10] as well as other non-military applications including crop monitoring and climate-change monitoring.[11] Generally, the weight of these cameras limits the operating range of the UAVs and usability in small arms fire control. The weight of these cameras is determined primarily by the associated optics. In all cases, reducing the weight of the optics would be highly advantageous to the effective utilization of UAVs, particularly for night-time surveillance. A similar problem exists in the case of arms- or body-mounted cameras as well. In this case, users (typically soldiers) have long complained about fatigue and health issues from the use of heavy cameras.[12] They are also highly detrimental to the situational awareness and agility of the soldiers in the scene of battle.

Conventional refractive optics is comprised of shaped surfaces and therefore tend to be bulky. These bend light based on the laws of refraction. Therefore, in order to achieve higher resolution (lower f# or larger field of view), one has to bend light at larger angles. This is achieved by making shapes with smaller radii of curvature. As a result, the optics tend to become thicker and heavier. This problem is highly exaggerated in the case of long focal lengths. Over the last 10 years, the Menon and the Sensale-Rodriguez labs at the University of Utah have developed an alternative approach exploiting multi-level diffractive optics.[1-5] Oblate Optics is now commercializing this technology. As described later, these novel flat optics can achieve the same performance as bulky refractive optics, but at a weight and volume that is up to 2 orders of magnitude smaller. For example, the weight of a conventional IR lens from Ophir Optics of diameter=28.5mm is 20grams, while that of a corresponding flat lens will be about 0.8grams, a factor of 25 times lighter. For larger aperture lenses, this disparity will be even higher. The market for imaging optics in general is rather large. According to a recent market study, IR optics is estimated to become a market of size $7.7 Billion in 2020.[13] We expect to have a significant commercial impact in this segment.

**Our Innovation**

In conventional optics, an ideal lens is one that imparts a *parabolic phase* on an incident wavefront of light, thereby converting an incident plane wave into a converging spherical wave. Such a strict phase requirement dictates that a single lens surface is unable to correct for image aberrations, including chromatic aberrations. Practically speaking, this means that most imaging systems require more than a single lens-surface. This leads to (1) thicker and (2) heavier cameras, (3) complexity in manufacturing due to requirement for precision alignment between multiple lenses, and (4) compromise in imaging performance (eg. operating bandwidth).

However, we recently discovered that this requirement of parabolic phase is not a strict constraint. In other words, we discovered a large number of phase functions that can all perform equally as a close-to-ideal lens.[1,2] This means that one can now apply various numerical methods to choose lens-phase distributions that are optimal for desirable properties such as achromaticity, minimize off-axis aberrations, manufacturability, etc. Since the lens is a ubiquitous component in all imaging systems, such a relaxation of design space has enormous implications for creating: (1) ultra-thin and (2) ultra-lightweight cameras, (3) drastically simpler assembly (due to the absence of precise alignments) and (4) almost no compromise in performance (eg. very large operating bandwidths).

Therefore, **our technical innovation is based upon (A) a fundamental discovery that the phase function of a lens is not unique.** A second innovation is (B) in the fabrication of such lenses, which require multi-level lithography at high resolution for high efficiency. We implemented these advancements in the form of multi-level diffractive lenses that can provide high efficiency and large operating bandwidths in a single surface as described next.

## Our solution

Our flat multi-level diffractive lenses (MDLs) are comprised of unit cells (or pixels), whose size is optimized to enable aberrations-minimized imaging. A photograph of an example MDL is shown in Fig. 1a. Since these pixels may be defined either as square pixels (Fig. 1b) or as concentric rings (Fig. 1c), this enables free-form optics or radial symmetry, respectively. A good overview of MDLs and comparison to alternative thin optics technologies is available in ref [14].

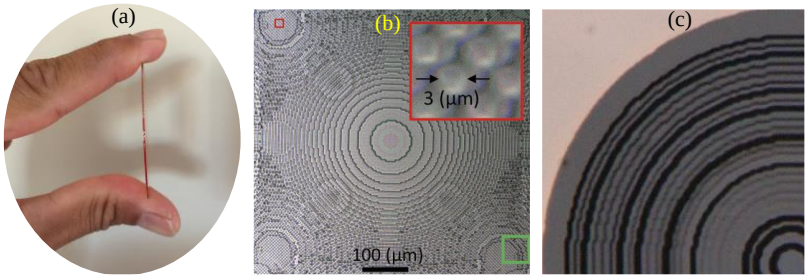


**Figure 1:Overview of MDLs. (a) Photograph showing an MDL fabricated in a 2.3um-thick polymer film atop a 0.6mm-thick glass wafer. Optical micrographs of a portion of (b) a free-form MDL and (c) a radially-symmetric MDL.**

The MDLs are designed via nonlinear optimization methods (such as gradient-descent assisted direct-binary search) that enables the choice of the MDL microstructure so as to minimize image (including chromatic) aberrations, while maintaining high focusing efficiencies. Our methodology also enables the direct application of fabrication tolerances, resulting in robust designs. Details of the design methodology have been described in these references.[1-5] The MDLs can be manufactured via imprint lithography at low cost and at high volumes.[8] The major steps are the fabrication of a master pattern and then the replication into daughter (final) patterns. The master pattern may be fabricated via multiple lithography and etch steps or via grayscale lithography (details are in these references [1-5]). The replication may be achieved in wafer-to-wafer, die-to-die or roll-to-roll processes. In each case, the imprinted polymer may be UV or thermal cured. The specific manufacturing process will be determined by the fabrication tolerance requirements of any given design. Oblate Optics has the capability to implement any of these required processes depending upon the design requirements.

**Summary of demonstrations:** MDLs have been experimentally demonstrated in all relevant spectral bands: visible,[1,15-17] near-IR,[5,7] SWIR,[4] MWIR,[1] LWIR[1-3] and THz.[18] More recently, we have even demonstrated a single MDL that is achromatic from the visible to the LWIR.[1] Exemplary images and corresponding MDLs are illustrated in Fig. 2. Recently, we have also shown that the MDLs can be designed for significantly larger depth-of-focus, which can remove the need for focusing mechanisms, potentially reducing SWAP even further.[19]

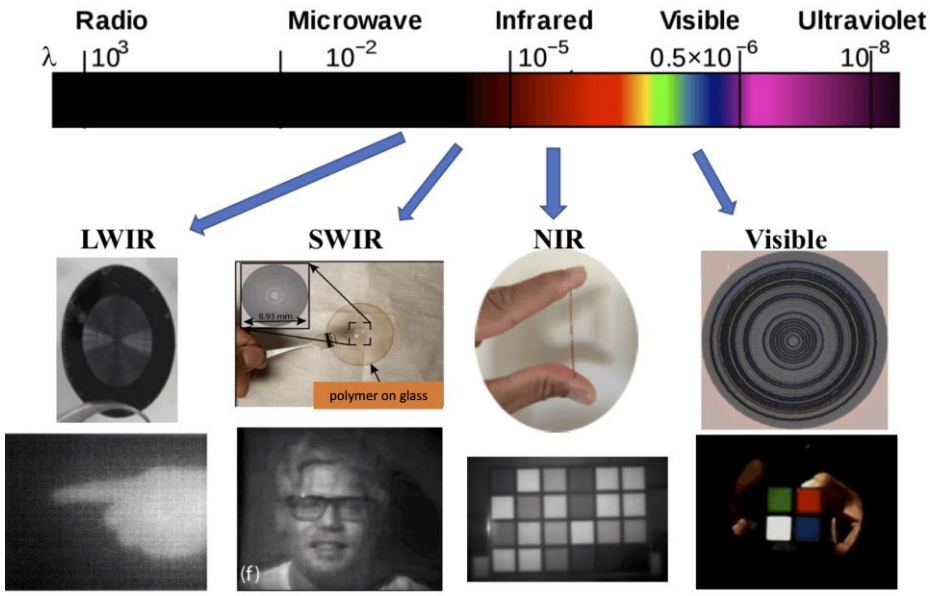


**Figure 2: Summary of experimentally demonstrated MDLs.**

**Note on scalability to large areas:** As described later, a new laser pattern generator (DWL66+ from Heidelberg Instruments) is being installed at the Univ. of UT via a DURIP grant in March 2020. We have discussed in detail with the tool manufacturer to estimate the write time needed for large-area flat lenses. Based on a 4-pass grayscale lithography process that we have previously developed, the estimated write time for 10 cm X 10cm area with minimum feature size of 0.8μm is expected to be about 3 days (73 hours). The largest area that can be written using the DWL66+ is 20cm X 20cm, but even larger areas could be accessed with larger tools manufactured by Heidelberg Instruments (for example, the VPG 1400 can write up to 1.4m X 1.4m). Even larger areas are, in principle, possible by stitching smaller areas together.

## Preliminary Results in the LWIR and MWIR (Broadband MDL)

We designed, fabricated and characterized example LWIR MDLs in a polymer material and the results are summarized in Fig. 3. The focal length and NA of the MDL is 8mm and 0.45. The simulated PSFs at the exemplary wavelengths are also shown. The simulations and simulated aberrations indicate close to diffraction-limited performance from λ=8μm to 12μm. The device was fabricated using grayscale lithography in a photopolymer atop a silicon wafer (see Fig. 3g,h). The MDL was coupled to a commercial LWIR image sensor to produce reasonable imaging results. This can be achieved, for example by improving the design algorithm, decreasing the minimum feature size, increasing maximum feature height and using a material with much lower absorption (like silicon).

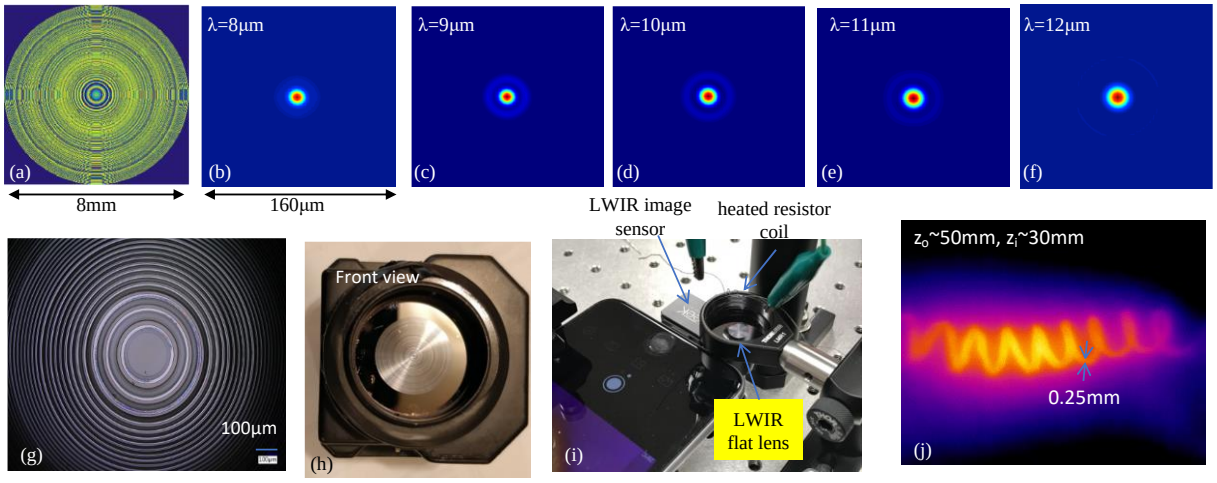


**Figure 3: Summary of preliminary LWIR MDL.[3] (a) Design. (b-f): Simulated PSFs. (g) Optical micrograph and (h) Photograph of fabricated device (polymer on Si). (i) Imaging setup with microbolometer array sensor. (j) Exemplary image of a heated resistor coil. $z_o$ and $z_i$ are the object and image distances, respectively.**

We also recently fabricated a MWIR lens (3μm to 5μm) with focal length of 25mm and f#/3 in a photopolymer film (thickness = 10μm) on a silicon wafer (Fig. 4a). This lens was shipped to L3Harris Technologies, where some preliminary imaging was performed (Fig. 4b).

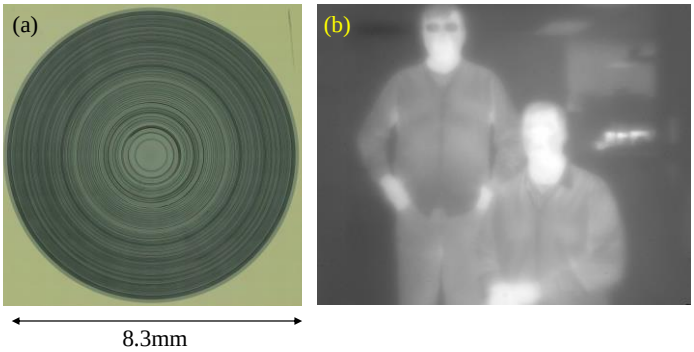


**Figure 4: Preliminary results from a MWIR MDL. (a) Optical micrograph of a fabricated MDL (photopolymer on silicon). (b) Image using this MDL (Courtesy of Dr. Nansheng Tang at L3Harris).**

Recently, we also demonstrated a single MDL that is achromatic from 0.45μm to 15μm.[1] We characterized the imaging behavior of the MDL by capturing still and video images of various objects. The results are summarized in Fig. 5. The field of view of the MDL is estimated as ~$15^0$. For majority of images, the distance between the MDL and the sensor was ~19mm for all wavelengths, and the distance between the MDL and the object was 450mm for the visible and NIR bands, and 425mm for the IR bands. In each case, the exposure time was adjusted to ensure that the frames were not saturated. In addition, a dark frame was recorded and subtracted from the images. For the images in the SWIR and longer wavelengths, a hot-plate at temperature of approximately $200^0$C was placed behind the objects in order to image their silhouettes. The only exceptions to this were the images of the soldering iron (3rd column in Fig. 5 at ~$180^0$C) and the heated resistor coil (only LWIR, 5th column in Fig. 6 at ~$150^0$C). The resolution-chart images in visible and NIR (Fig. 5) shows that the resolved spatial frequency is ~28.5 line-pairs/mm, which corresponds to a spatial period of ~17.5μm or about ~8 times the sensor pixel size (2.2μm). This resolution corresponds approximately to the average FWHM over the visible-NIR bands. We also note that the visible image of the Macbeth color chart shows excellent color reproduction.

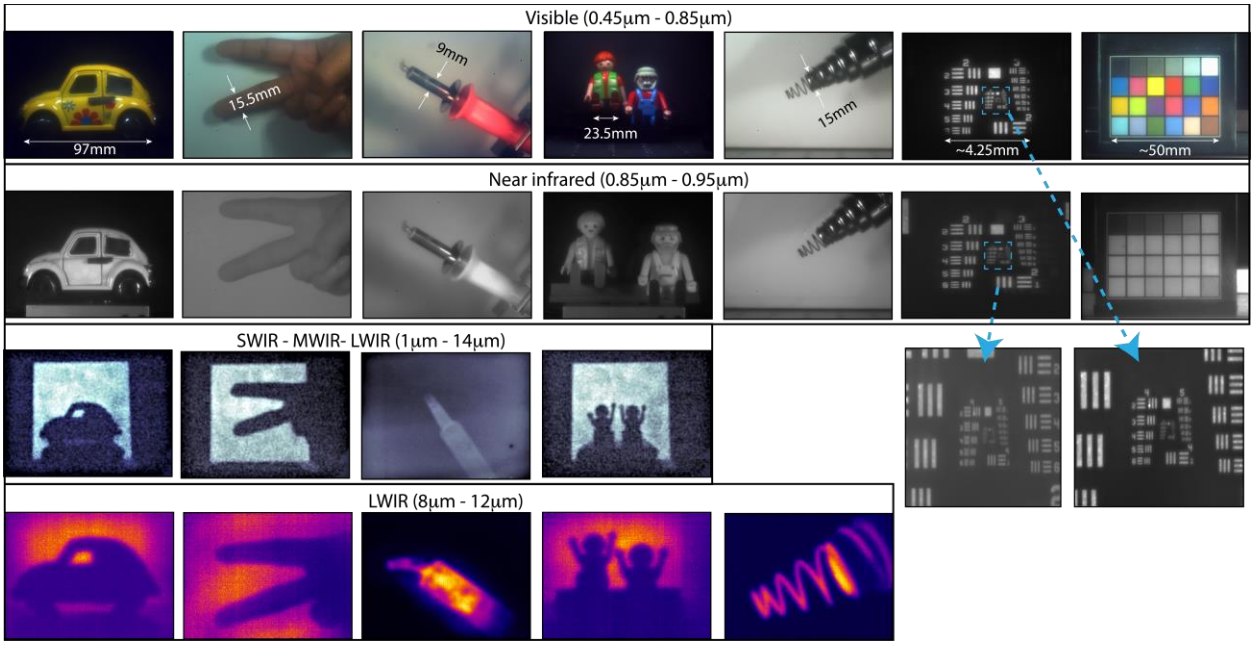


**Figure 5: Imaging from the visible to the LWIR using a single MDL. The visible and NIR images were taken using the silicon CMOS image sensor. The LWIR images were taken using a FLIR Tau2 camera sensor. The remaining images used the BST microbolometer focal plane array. The MDL with glass substrate was used for visible and NIR wavelengths, while the MDL with Si substrate was used for all other wavelengths. Note that all images are raw and unprocessed. Also see corresponding videos in Supplementary Videos 1-8. Note that for the SWIR-MWIR-LWIR images, the lower wavelength cut-off arises from transmission of the silicon substrate, and no filters were used. Work performed in collaboration with Dr. Philip Hon at Northrop Grumman.**

## Aberrations Performance

Using simulations, we characterized the lens aberrations of the LWIR MDL as summarized in Fig. 6(a) at λ=8μm, and confirmed that the aberrations are very low and comparable to more complex lens systems. We have also experimentally measured the wavefront aberrations of a visible-NIR MDL and confirmed the excellent performance as summarized in Figs. 6(b) and (c).

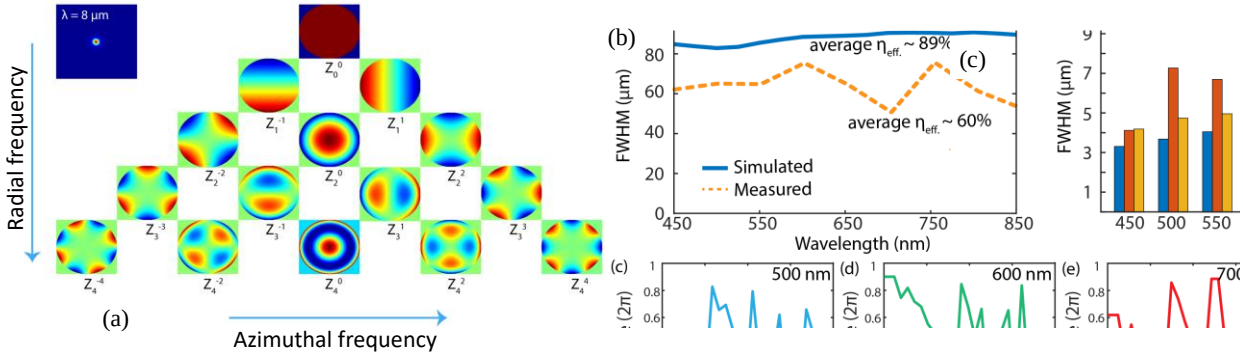


**Figure 6: The MDL has excellent aberrations performance. (a) Simulated aberrations coefficient of the LWIR MDL shown in Fig. 3. (b) Experimentally obtained aberrations coefficients for a visible-NIR MDL, also compared to a conventional refractive (stock) lens from Thorlabs. (c) Measured wavefront of this MDL under broadband visible illumination.**

It is also possible to design the MDL to dramatically reduce off-axis aberrations, for example to enable large field-of-view (FOV) compared to conventional lenses. An example is shown in Fig. 7, where the MDL was designed to obtain a FOV of ~100deg. In this example, both chromatic and off-axis aberrations were minimized.

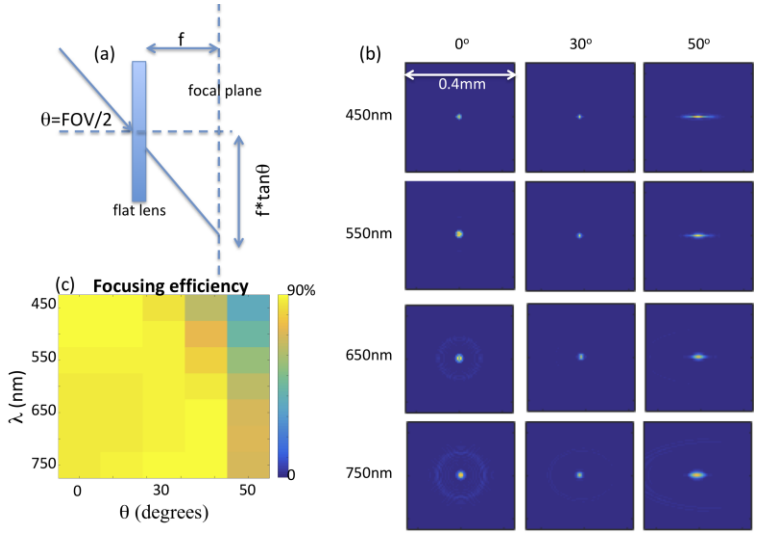


**Figure 7: Off-axis performance. (a) The MDL can be designed to minimize off-axis aberrations to enable large FOV. Simulated (b) PSFs and (c) focusing efficiency of one such visible MDL with FOV ~100$^0$.**

## High-NA (low-f#) lenses

It is important to emphasize that MDLs with low f# are indeed possible.[7] In Fig. 8, we show an example of an MDL with NA=0.9 (f#=0.24) with close-to-diffraction-limited performance.

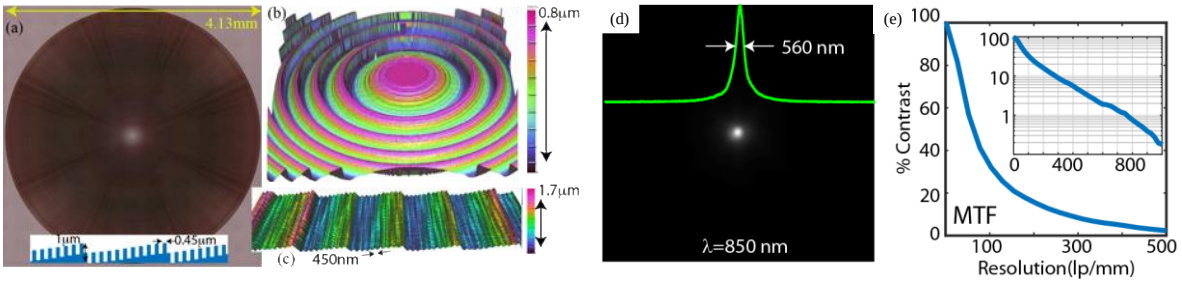


**Figure 8: MDL with NA=0.9 (f#=0.24). (a) Optical micrograph, and 3D confocal image of (b) inner rings and (c) outer rings. (d) Measured PSF. (e) Measured MTF.**

## Comparison to metalenses

Recently, planar metalenses have been used for imaging.[20,21] Unfortunately, metalenses require subwavelength features and large aspect ratios, making them impractical for low-cost manufacturing over large areas. In addition, they usually suffer from polarization sensitivity[22-24] and possess significant chromatic aberrations.[25-28] Metalenses with conical wavefronts have been demonstrated for focusing.[29,30] However, these suffer from relatively low transmission efficiency, require very small features (<100nm) and therefore are difficult to scale to larger apertures. Recently, we demonstrated that metalenses are not required for imaging light intensities, a scalar property of the electromagnetic field. Diffractive optics with super-wavelength features and relatively low aspect ratios, which are far simpler to fabricate, are sufficient for imaging light intensities. However, we note that metasurfaces are required to manipulate vector properties of light such as polarization. We further emphasize that we previously demonstrated water-immersion diffractive lenses with numerical aperture (NA) as high as 1.43.[6] We summarize the key differences between our lenses and the recently demonstrated metalenses in Table 1 below.

**Table 1: Comparison between MDLs and metalenses**.

| **Parameter** | **MDL** | **Metalens** |
|---|---|---|
| Smallest feature width | > ~0.5μm | < ~0.06μm |
| Maximum feature height | ~2.5μm | ~0.8μm |
| Largest aperture shown so far | 1cm diameter | 0.022cm diameter |
| Polarization sensitivity | None | Generally sensitive |
| Bandwidth shown so far | 400nm | 200nm |
| Can be imprinted in polymer | Yes | No (needs high index like $TiO_2$) |

## Comparison to conventional optics

Conventional refractive lenses are the dominant incumbent technology. These tend to be thick and their thickness and weight increase with increasing field of view. Conventional diffractive lenses (like Fresnel lenses) tend to operate in a narrowband spectrum and are not applicable for vast majority of imaging applications. A summary of the differences between the Oblate flat lenses and conventional refractive and diffractive optics is in Table 2.

**Table 2: Compare Oblate Flat Lens to conventional Refractive and Diffractive lenses.**

| ***Figure of Merit*** | ***Oblate Flat Lens*** | ***Conventional Refractive Lens*** | ***Conventional Diffractive Lens*** |
|---|---|---|---|
| ***Thin & lightweight*** | *Yes* | *No* | *Yes* |
| ***Multiple lenses required*** | *No* | *Yes* | *Yes* |
| ***Image aberrations corrected*** | *Yes* | *Yes with multiple lenses* | *No* |
| ***Operating bandwidth*** | *Large (eg. full visible)* | *Large (eg. full visible)* | *Small (narrowband)* |
| ***Wide FOV*** | *Yes* | *Yes with thick lenses* | *No* |
| ***Very Low-cost manufacturing*** | *Yes* | *No* | *Yes* |

Finally, in Fig. 9, we summarize our preliminary experiments using two MDLs in tandem for focus adjustment.[15] By adjusting the distance between the two lenses, it is possible to change the effective focal length (as with conventional refractive lenses).

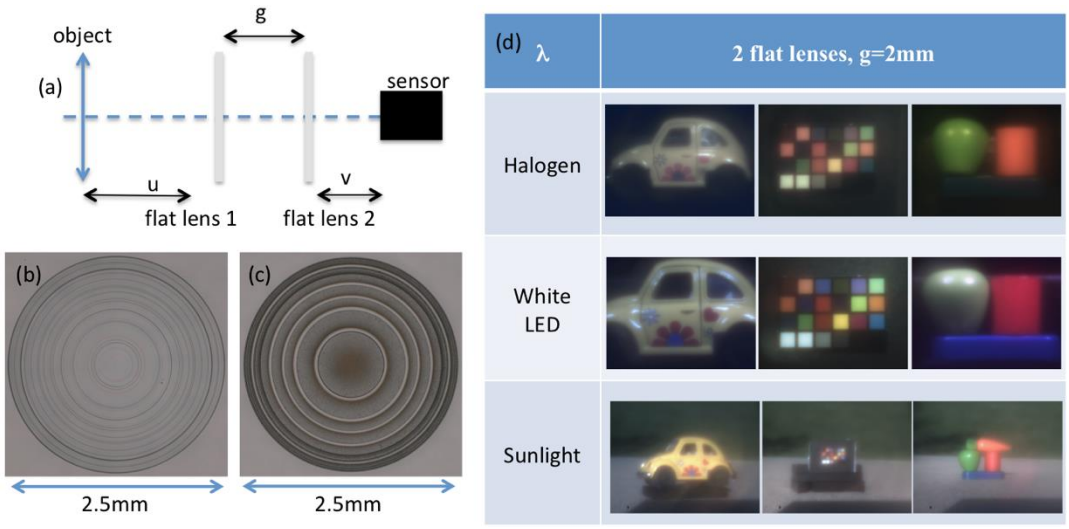


**Figure 9: Preliminary experimental results using the 2 flat lenses in tandem. (a) Schematic. (b), (c) Optical micrographs of fabricated flat lenses. (d) Color images taken with two flat lenses and the color CMOS image sensor under different illumination conditions.**

## Technical Objectives

In this effort, Oblate Optics performed the design, fabrication and characterization of a MWIR (3μm to 5μm) flat lens that can be utilized with the curved focal-plane array being developed under the DARPA FOCII program. One of the goals of the program was to achieve very wide field of view imaging of at least 120$^{o}$ full angle. Specifically during the base period, we performed optimization-based inverse design and numerical verification of a flat lens with operating wavelength in the MWIR band, f# = 2 and focal length of 20mm.

**Table 3: Parameters for POC MDL.**

| | **Base** | **Option** *(note the option was not selected for funding)* |
|---|---|---|
| Clear aperture (diameter) | 10mm | 25mm |
| Effective focal length | 20mm | TBD |
| Object space numerical aperture / f# | 0.2425/ f#2 | TBD |
| Wavelengths of operation | 3mm to 5mm | |
| Material | Patterned Si | Patterned Si (or Ge) |
| Size | Can be diced to specification | |
| Thickness | <= 0.6mm | |
| Weight per lens | < 1g | |
| Wmin / Hmax (approx.) | 5μm / 10μm | TBD |

## 3. Methods, Assumptions, and Procedures

### Update design software: off-axis PSFs

One of the big challenges of designing the flat lenses is the computational complexity of our approach. Since we use an iterative direct-binary-search algorithm to optimize the geometry of the flat lenses, it requires significant computational time, especially to design larger-aperture lenses. This is particularly true in the case of large angles of incidence or off-axis PSFs as is required in this effort. Therefore, our first task was to develop techniques to increase the computational efficiency of this search process.

Although a direct binary search technique (DBS) can yield designs with good performance metrics, such search techniques are however, limited by their exponential time complexity in an unstructured design solution space. If the solution can be proven to exist, we can further perform a gradient descent optimization along with the binary search to overcome the time complexity required to arrive at the desired solution.

A second approach to reduce computational speed is to take advantage of symmetry and also parallel processing. Since the flat lenses are comprised of concentric rings, the problem is essentially reduced to a 2D problem. However, solving the scalar diffraction propagation with cylindrical symmetry requires the use of Hankel transforms, which are generally slower than 2D Fast Fourier Transforms (which are required for full 3D simulations). Therefore, it is not simple to take the conventional scalar-diffraction model and apply cylindrical symmetry to it. However, an alternative simple approach exists, which is to design a 1D lens that forms a line focus first. Then, simply apply a body-of-revolution methodology to convert the 1D lens into a 2D circular-symmetric lens. We modified our software to achieve this symmetry, which offered a significant speedup compared to the previous methods. We have already implemented finite-difference time-domain (FDTD) models for normal incidence that take advantage of rotational symmetry. Here, we will extend this prior work to large angles of incidence. Of course, for design purposes this has to be done with scalar models, but verification can be achieved with FDTD.

### Update design software: non-planar FPA

Since the FOCI program is developing a curved FPA, we adapted our design software to ensure that we can compute the PSF on a curved surface as illustrated in Fig. 10. By applying the rotational symmetry about the optical axis, we can speed up the computation.

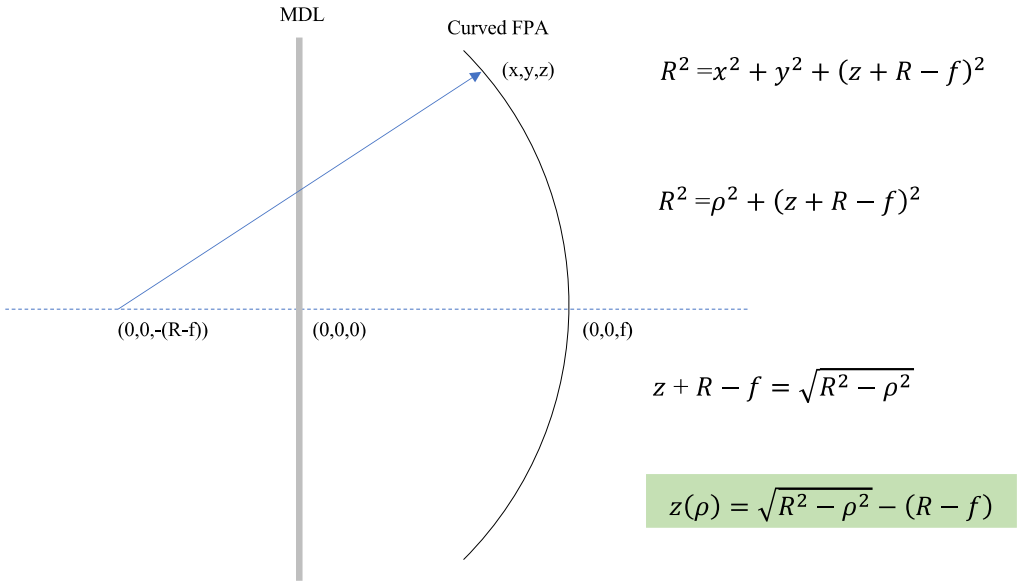


**Figure 10: Schematic of MDL imaging onto a curved FPA. The radius of curvature of the FPA is exaggerated for clarity.**

## Code V integration package:

CODE V optical design software (Synopsis, Inc.) is a computer aided design software used to model, analyze, optimize, and provide fabrication support for the development of optical systems in the regime of geometrical optics (ray tracing). This tool is widely used by optical designers in all industries. We created a package to integrate the output of our software (which is the complex field as a function of space and wavelength) into the existing Code V engine, which will enable a seamless illustration of the performance of our flat lenses in a format that is easily recognizable by the vast majority of optical designers. This integration was validated with several test lens designs, and also with experimental data.

## Parametric Studies:

We further used the numerical models described above to study the impact of the radius of curvature of the sensor on the performance of the flat lens. The results are described in the next section.

## Fabricate POC flat lens with multi-litho and etch process.

The master pattern itself was fabricated via multiple (aligned) lithography steps (where each litho is followed by an etch). Details of this process are illustrated in Fig. 11. Only 2 steps are shown, but with N such steps, $2^N$ final levels can be patterned. The key challenge during this process are the overlay accuracy for each step. Finally, replication at high aspect ratios could

also be challenging. The replication step was proposed for the option period, which was not undertaken.

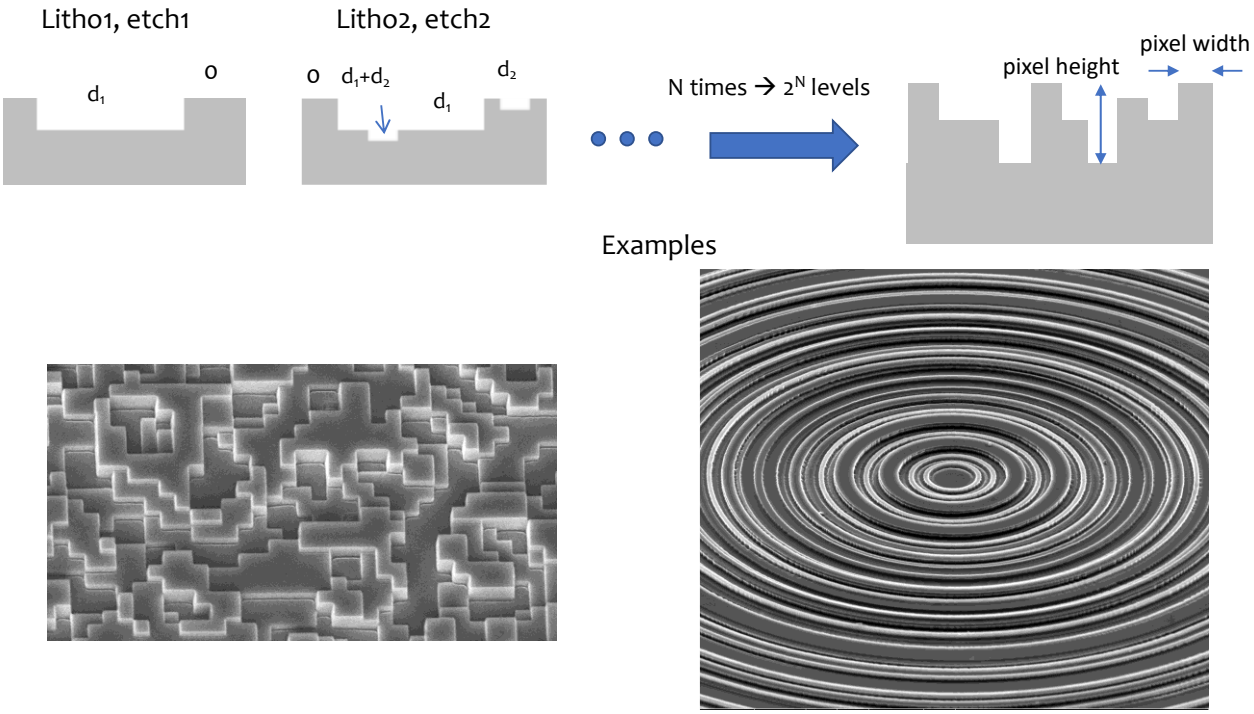


**Figure 11: Fabrication process. The device is created by repeated (aligned) lithography and etch steps. With N steps, one can attain 2N levels. Scanning-electron micrographs of two examples made in silicon are shown.**

## Characterization:

Finally, we performed characterization of the lenses using a tunable quantum-cascade laser as the light source and measured the point-spread functions, as well as performed simple imaging experiments.

## 4. Results and Discussion

### POC Design

We used the inverse-design tool described earlier to create the proof-of-concept (POC) design assuming material = Silicon, ring-width = 1µm, maximum ring height = 3µm and 32 levels of height. The geometry of the chosen design is shown in Fig. 12.

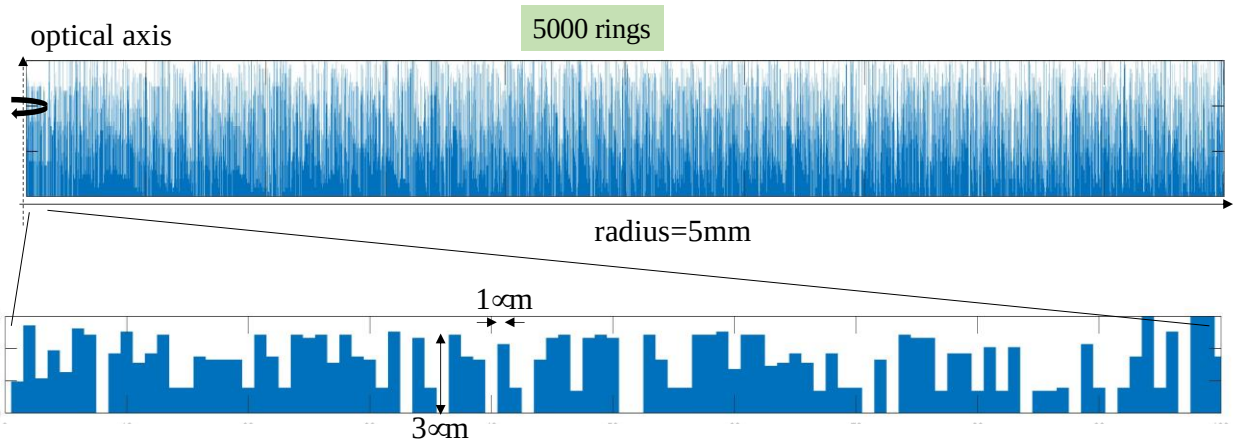


**Figure 12: POC (Base) design in silicon containing 5000 rings.**

**Table 4: Parameters of the flat lens.**

| | 1st 11 months | Next 12 months | Fabricated |
|---|---|---|---|
| Clear aperture (diameter) | 10mm | 25mm | 25.4mm |
| Effective focal length | 20mm | TBD | 27.94mm |
| Object space numerical aperture / f# | 0.2425/ f2 | TBD | 0.41/f1.1 |
| Wavelengths of operation | 3µm to 5µm | | |
| Material | Patterned Si | Patterned Si (or Ge) | Patterned Si |
| Size | Can be diced to specification | | 26mm X 26mm |
| Thickness | <= 0.6mm | | 0.55mm |
| Weight per lens | < 1g | | =0.471g |
| Wmin / Hmax | 1µm / 3µm | TBD | 1µm / 3µm |
| FOV | ∓50⁰ | | |

**Weight (including substrate) = 0.471g.**

**Simulations and parametric study**

We used the models to simulate the point-spread function of the flat lens at different illumination wavelengths and incident angles as summarized in Fig. 13 for the case of the flat image sensor.

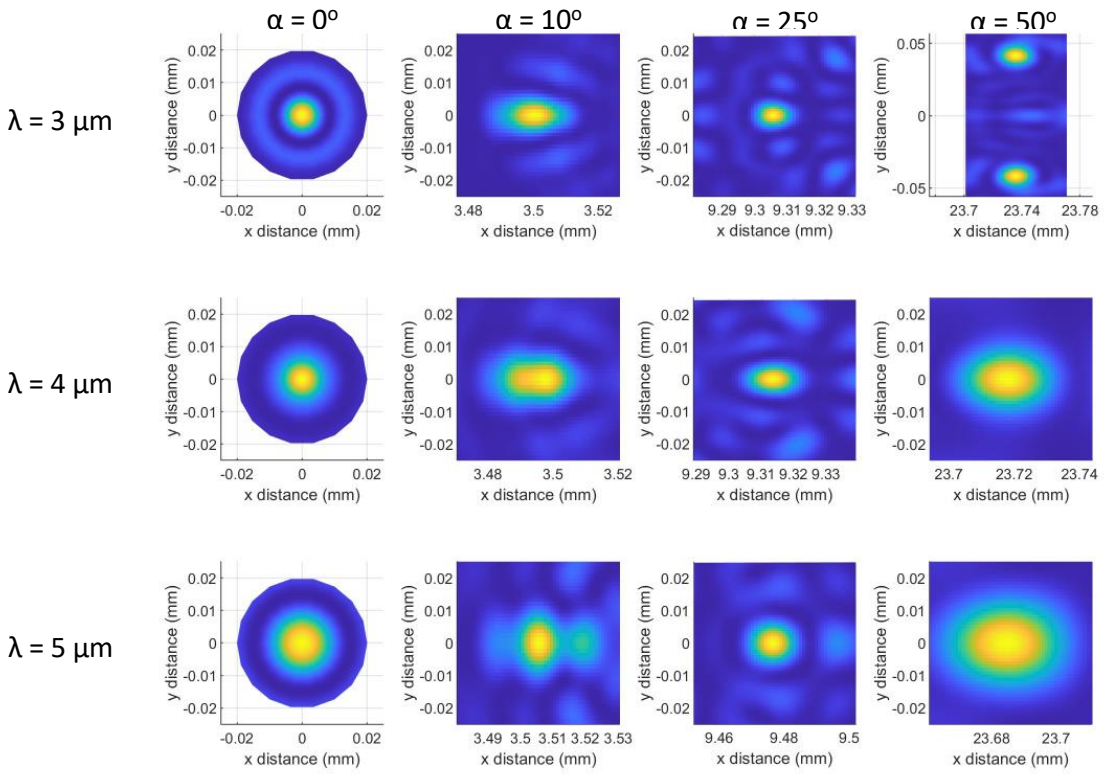


**Figure 13: Simulated PSFs for the flat image sensor.**

Additional designs were performed for various radii of curvature of the image sensor to showcase the parametric study. These are summarized in Figures 14-19 below for sensor different radii of curvature.

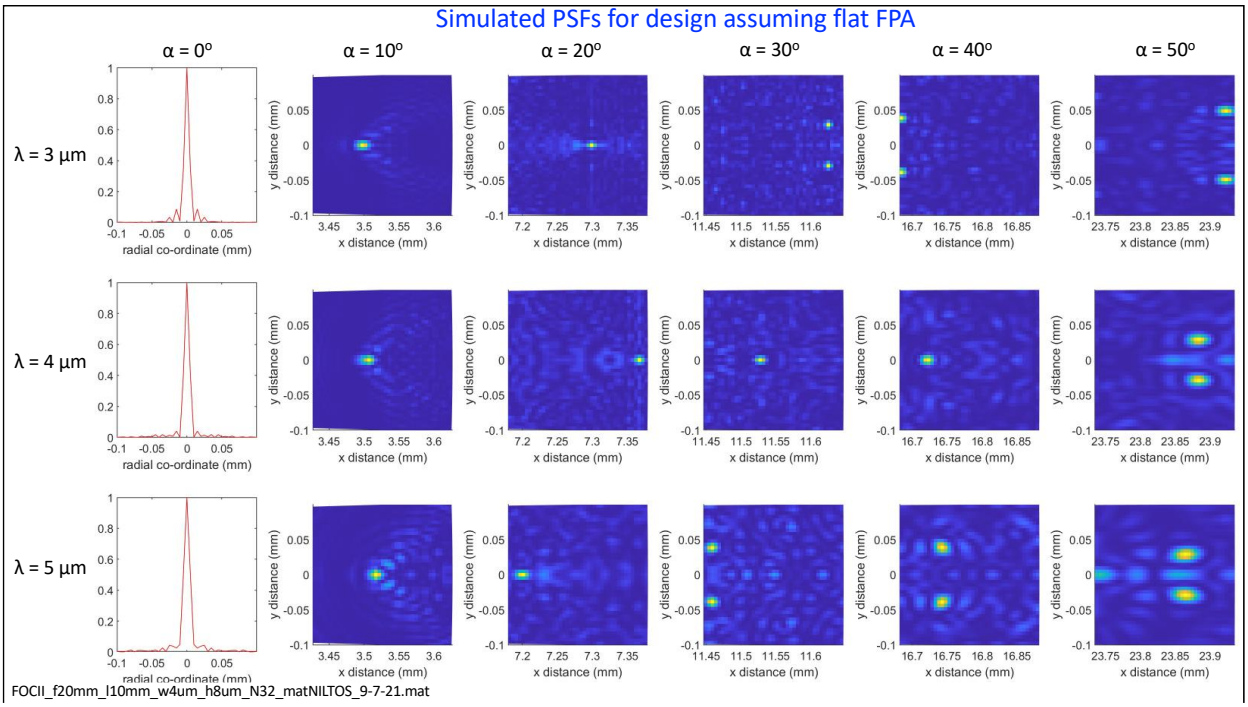


**Figure 14: Simulated PSFs for a flat FPA with a larger range.**

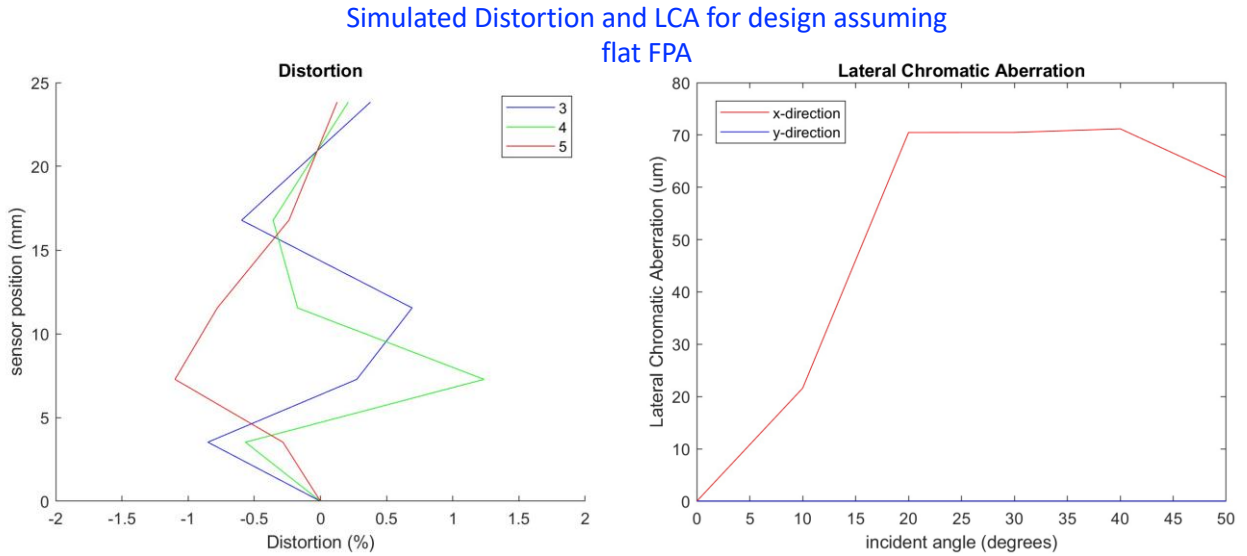


**Figure 15: Simulated aberrations (distortion and lateral chromatic aberrations) for the flat FPA.**

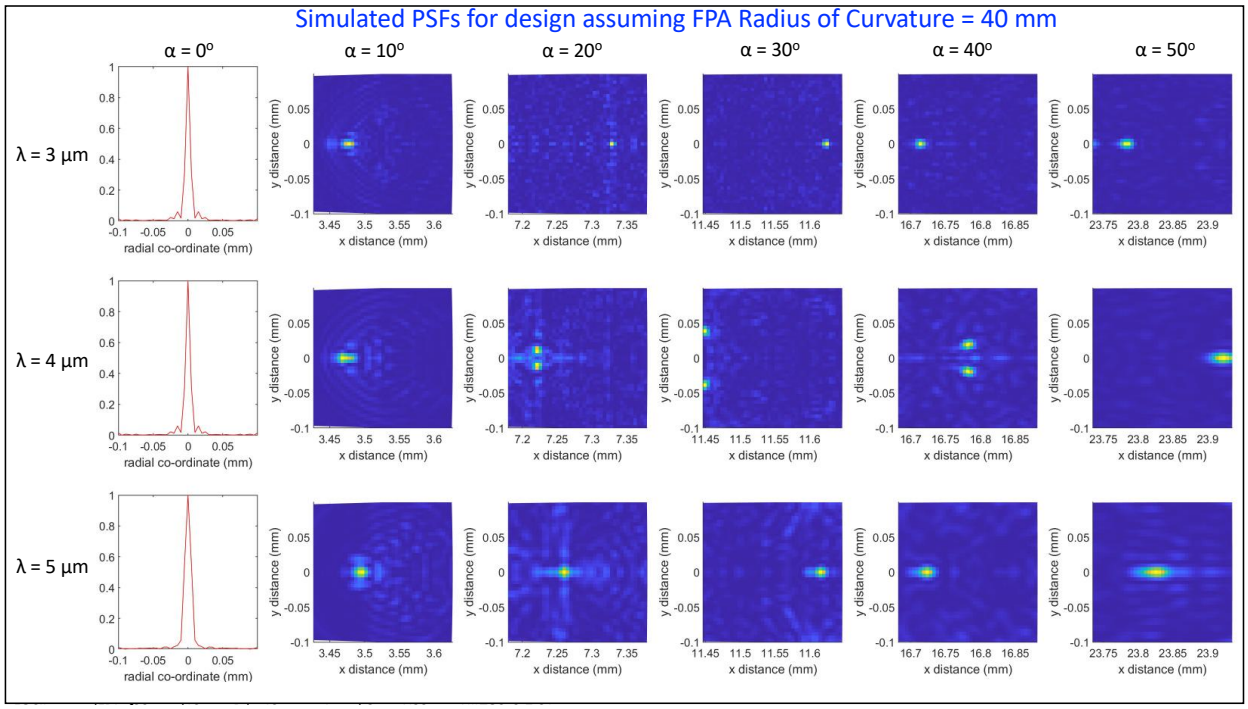


**Figure 16: Simulated PSFs for a FPA with radius of curvature = 40mm.**

Simulated Distortion and LCA for design assuming
FPA Radius of Curvature = 40 mm

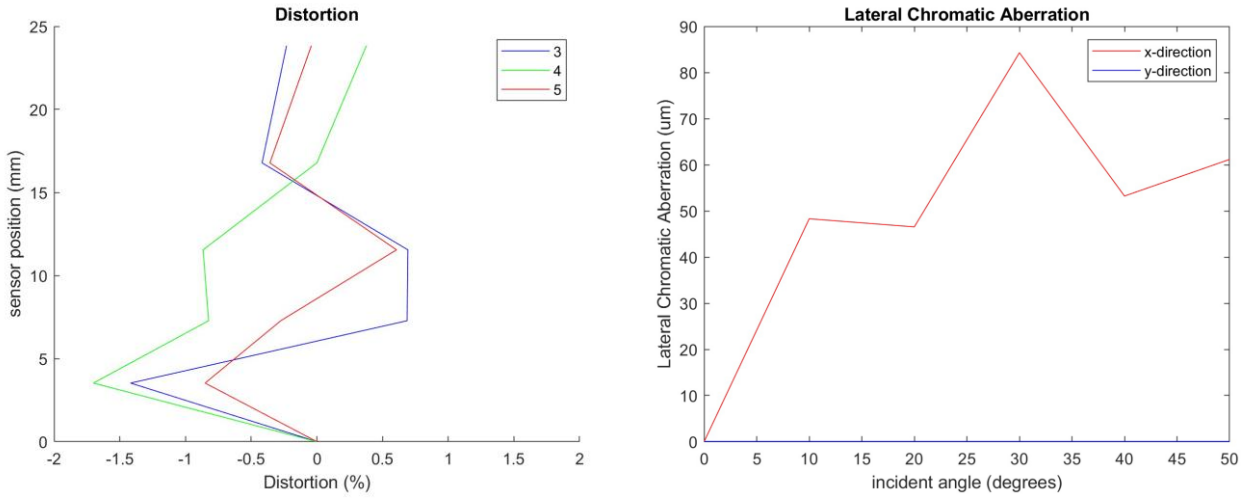


**Figure 17: Simulated aberrations (distortion and lateral chromatic aberrations) for a FPA with radius of curvature = 40mm.**

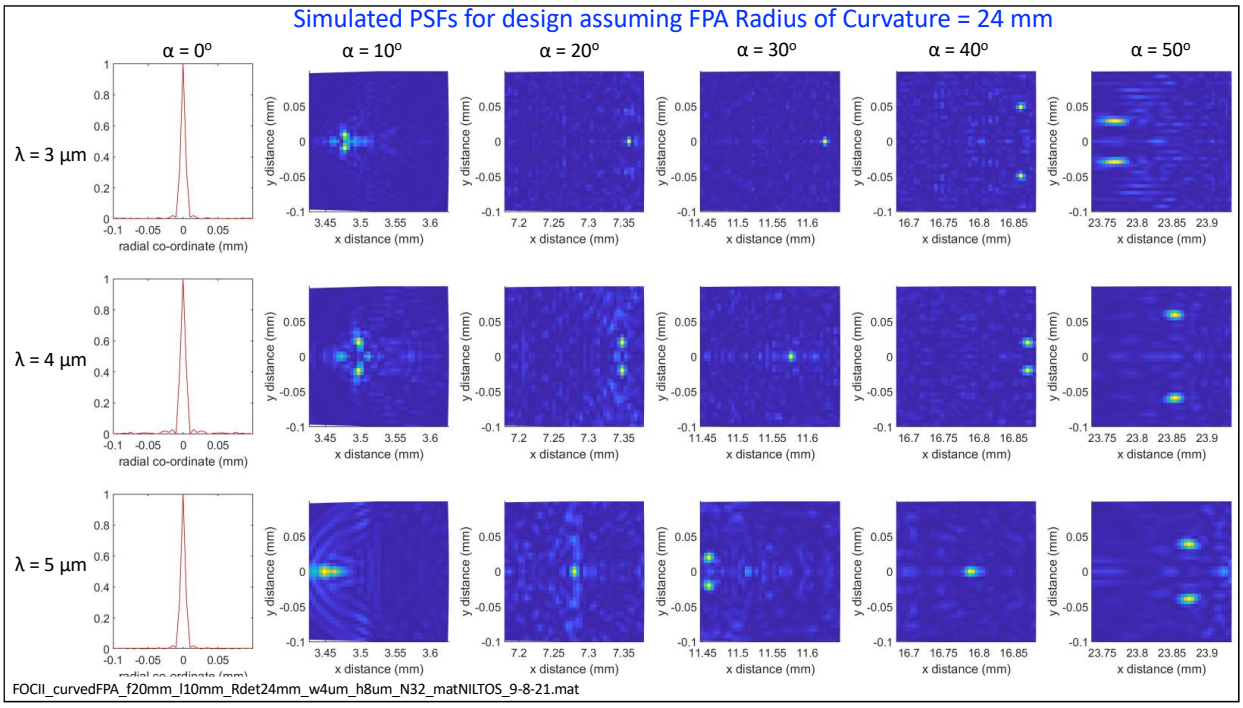


**Figure 18: Simulated PSFs for a FPA with radius of curvature = 24mm.**

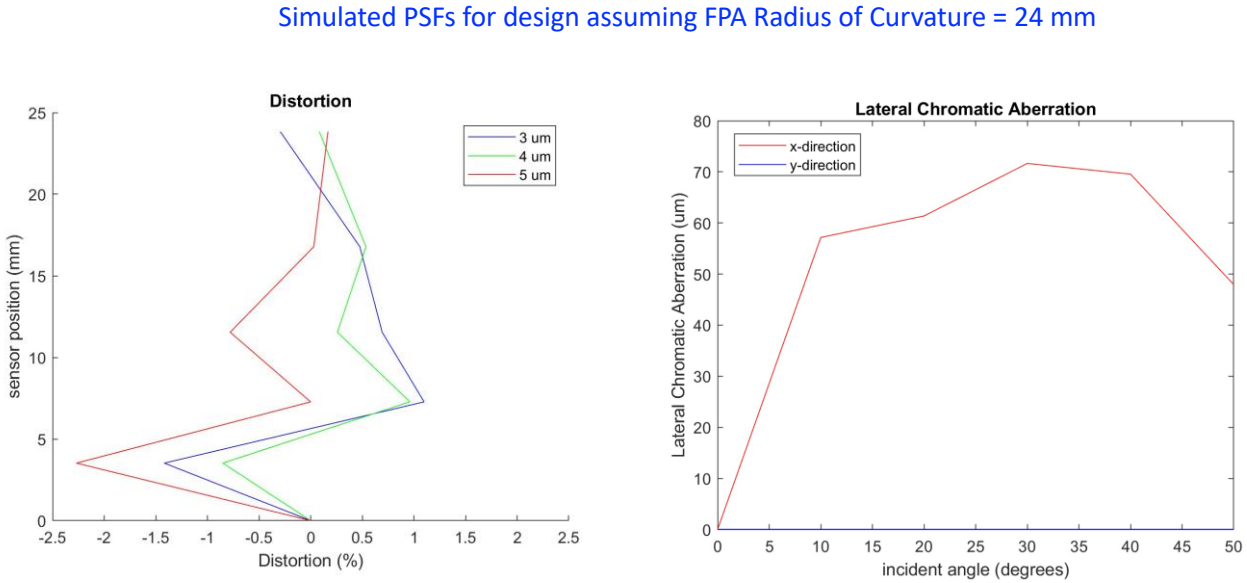


**Figure 19: Simulated aberrations (distortion and lateral chromatic aberrations) for a FPA with radius of curvature = 24mm.**

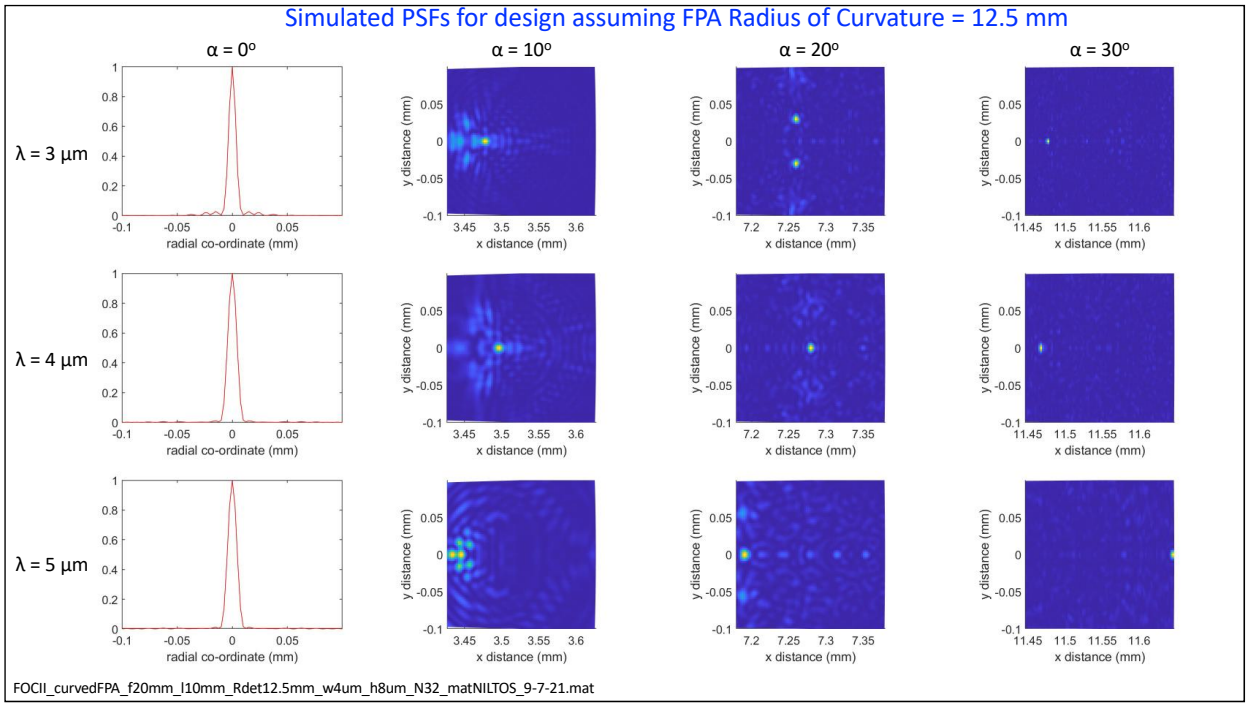


**Figure 20: Simulated PSFs for a FPA with radius of curvature = 12.5mm.**

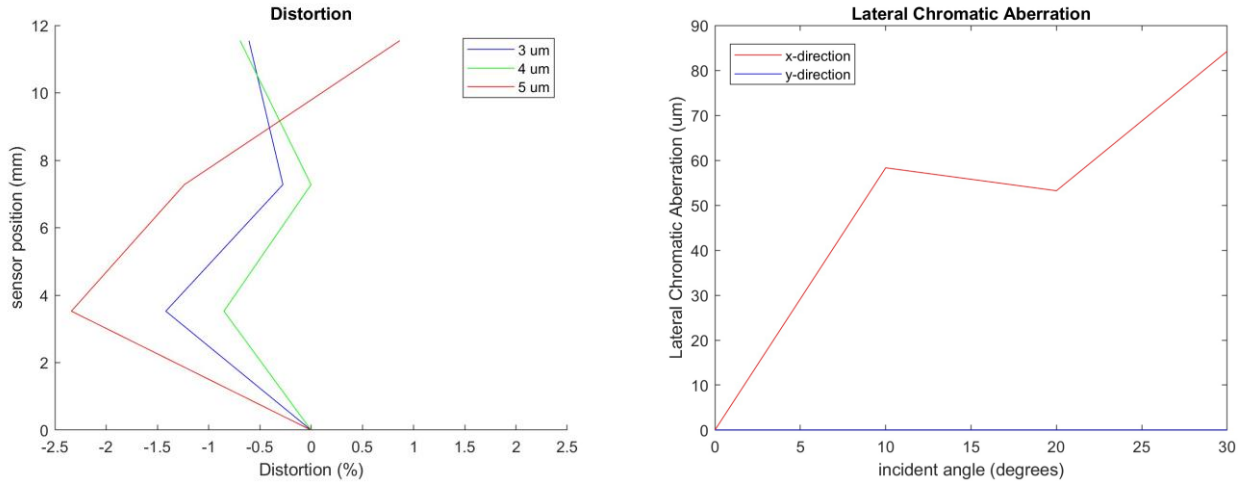


**Figure 21: Simulated aberrations (distortion and lateral chromatic aberrations) for a FPA with radius of curvature = 12.5mm.**

The main conclusions of this parametric study were:

- Focusing over the full FOV is not strongly affected by the radius of curvature eof the FPA.

- Curved FPAs can improve the relative illuminance and can especially be useful for pixels with small acceptance angles.

Fabricated Devices

The devices were fabricated using the multiple lithography and etch steps described earlier. A photograph of one wafer containing 4 lenses is shown in Fig. 22.

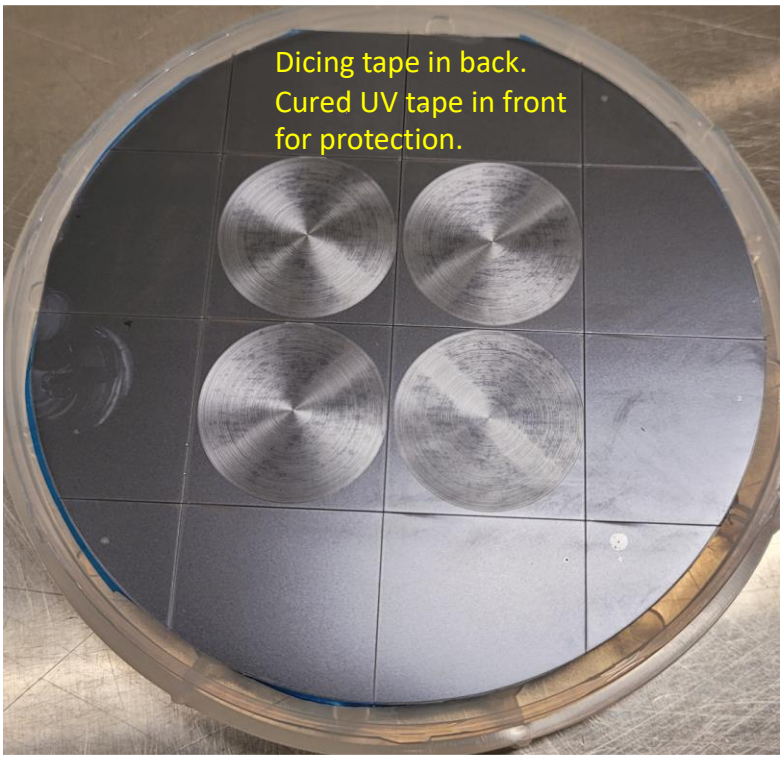


**Figure 22: Photograph of fabricated devices.**

The fabricated devices were characterized using scanning confocal microscopy to measure their 3D profiles (see Fig. 23). We compared the measured values to the design and obtained a standard deviation of errors of about 2μm.

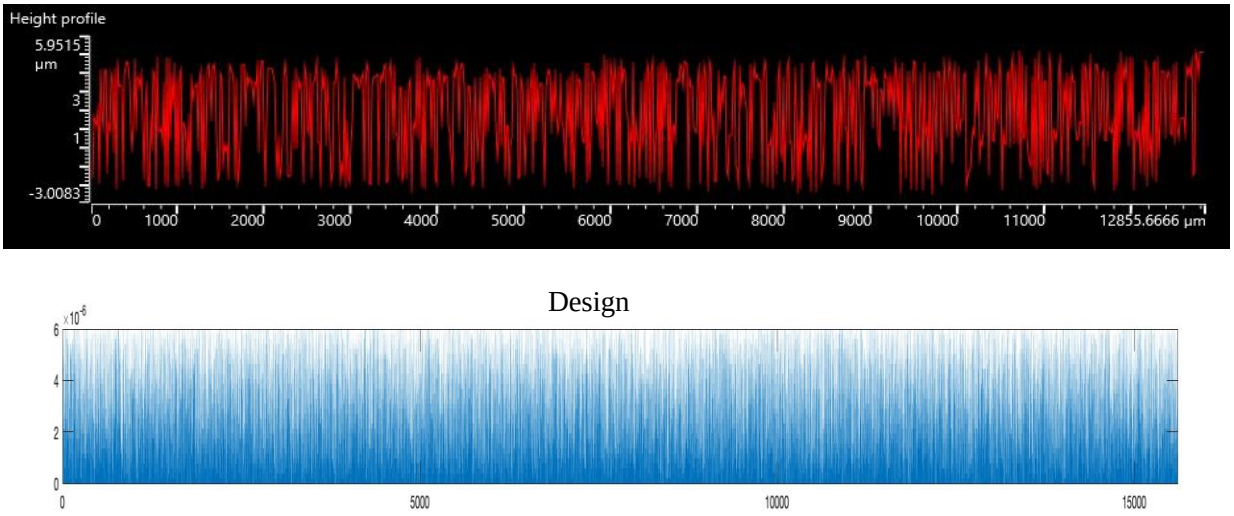


**Figure 23: Measured ring-heights from the fabricated device (top) and design (bottom).**

## Imaging Experiments:

We used a hot plate as the self-luminous source and placed various objects to create shadows in front of the source for imaging. The results are shown in Fig. 24. The sensor used was an Electrophysics sensor with pixel size of 40µm. This sensor has sensitivity to photons of wavelength from 1µm to 14µm. No filter was used in these experiments, so the background (unfocussed) light is expected to be high. No post-processing was performed.

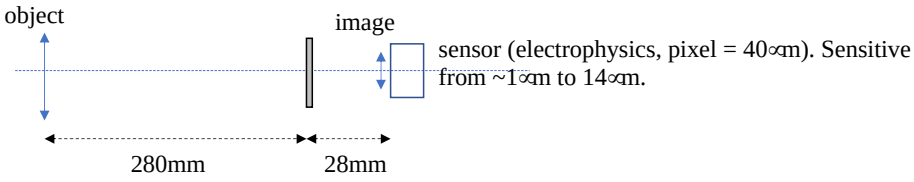


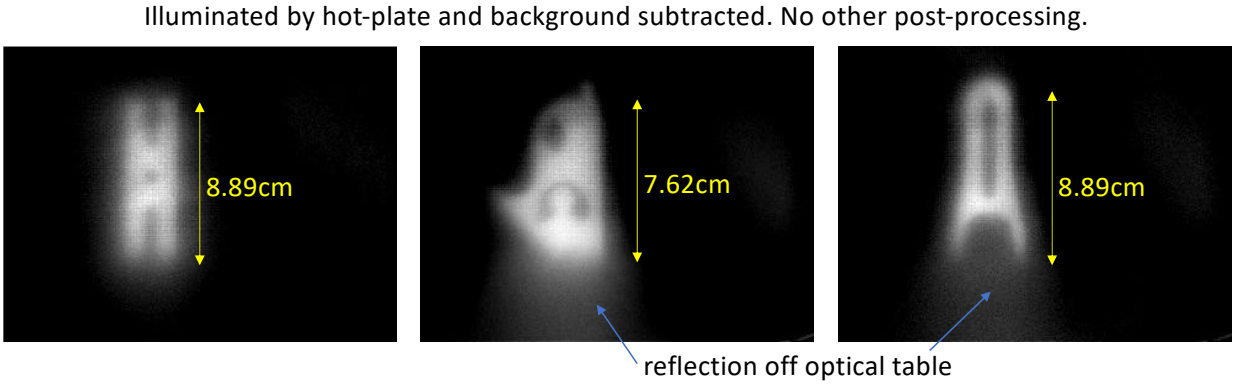


**Figure 24: Imaging Experiments.**

We also performed a second experiment to estimate the FOV of the lens as summarized in Fig. 25 below.

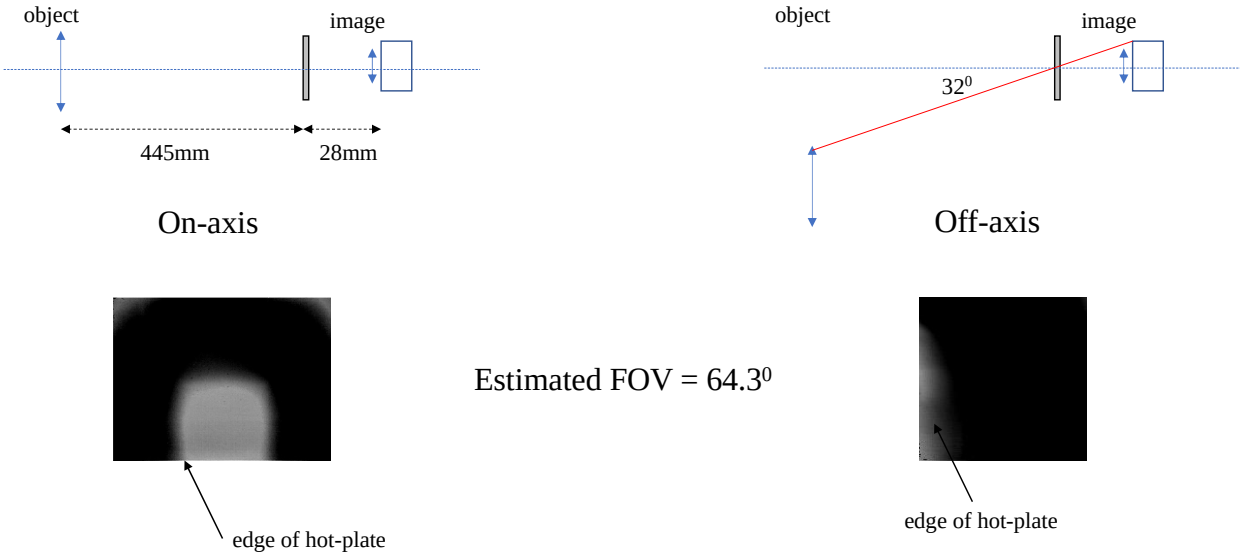


**Figure 25: The object was moved across the FOV of the lens to estimate its FOV as illustrated.**

## 5. Conclusion

This base study indicated that flat lenses have significant potential in attaining lightweight large FOV optics in the MWIR. Unfortunately, the option effort was not funded, so optimal design, fabrication and full set of characterization experiments could not be completed. Nevertheless, this effort successfully laid the software groundwork for future design and fabrication efforts.

## 6. References


1. M. Meem, S. Banerji, A, Majumder, P. Hon, J. C. Garcia, B. Sensale-Rodriguez & R. Menon, "Imaging from the visible to the longwave infrared via an inverse-designed flat lens," arXiv:2001.03684 [physics.optics] (2020).

2. S. Banerji, M. Meem, A. Majumder, B. Sensale-Rodriguez & R. Menon, "Imaging over an unlimited bandwidth with a single diffractive surface," Open-access version: arXiv:1907.06251 [physics.optics] (2019).

3. M. Meem, S. Banerji, A, Majumder, F. G. Vasquez, B. Sensale-Rodriguez & R. Menon, "Broadband lightweight flat lenses for longwave-infrared imaging," *Proceedings of the National Academy of Sciences* Oct 2019, 201908447 (2019).

4. M. Meem, S. Banerji, A. Majumder, C. Dvonch, B. Sensale-Rodriguez & R. Menon, "Imaging across the Short-Wave Infra-Red (SWIR) Band via a Flat Multilevel Diffractive Lens," *OSA Continuum* 2 (10) 2968-2974 (2019)

5. S. Banerji, M. Meem, A, Majumder, F. Vasquez-Guevara, B. Sensale-Rodriguez & R. Menon, "Ultra-thin near infrared camera enabled by a flat multi-level diffractive lens," *Opt. Lett.* 44(22) 5450-5452 (2019).

6. D. Chao, A. Patel, T. Barwicz, H. I. Smith, and R. Menon, "Immersion Zone-Plate-Array Lithography," J. Vac. Sci. Technol. B, 23(6), 2657-2661 (2005).

7. M. Meem, S. Banerji, C. Pies, T. Oberbiermann, B. Sensale-Rodriguez & R. Menon, "Large-area, high-NA multi-level diffractive lens via inverse design," *Optica* (*in press*).

8. Guo, L. J. Recent progress in nanoimprint technology and its applications. *J. Phys. D: Appl. Phys.* **37** R123-R141 (2004).

9. A. C. Watts, V. G. Ambrosia, and E. A. Hinckley, "Unmanned Aircraft Systems in Remote Sensing and Scientific Research: Classification and Considerations of Use," *Remote Sensing* 2012, *4*(6), 1671-1692; doi:10.3390/rs4061671.

10. M. Vollmer and K. P. Moellmann, "Infrared thermal imaging: Fundamentals, Research and Applications," Wiley-VcH (2018).

11. L. P. Koh and S. A. Wich, "Dawn of Drone Ecology: Low-Cost Autonomous Aerial Vehicles for Conservation," Tropical Conservation Science 5(2), 121-132 (2012).

12. S. J. Manoogian, E. A. Kennedy and S. M. Duma, "A Literature Review of Musculoskeletal Injuries to the Human Neck and the Effects of Head-Supported Mass Worn by Soldier," Defense Technical Information Center, ADA441139 (2005).

13. Night vision device market report by Markets and Markets: https://www.marketsandmarkets.com/PressReleases/night-vision-device.asp

14. S. Banerji, M. Meem, B. Sensale-Rodriguez and R. Menon, "Imaging with flat optics: metalenses or diffractive lenses?," *Optica* 6(6) 805-810 (2019).

15. M. Meem, A. Majumder and R. Menon, "Full-color video and still imaging using two flat lenses," *Opt. Exp.* 26(21) 26866-26871 (2018).

16. P. Wang, N. Mohammad and R. Menon, "Chromatic-aberration-corrected diffractive lenses for ultra-broadband focusing," *Nature Scientific Reports* 6, 21545 (2016).

17. N. Mohammad, M. Meem, B. Shen, P. Wang and R. Menon, "Broadband imaging with one planar diffractive lens," *Sci. Rep. 8 2799* (2018).

18. S. Banerji, B. Sensale-Rodriguez, A Computational Design Framework for Efficient, Fabrication Error-Tolerant, Planar THz Diffractive Optical Elements. Sci. Rep. 9, 5801 (2019).

19. Banerji, M. Meem, A, Majumder, B. Sensale-Rodriguez & R. Menon, "Diffractive flat lens enables Extreme Depth-of-focus Imaging," *Optica* (*in press*).

20. Arbabi, A., Arbabi, E., Kamali, S. M., Horie, Y., Han, S. and Faraon, A. Miniature optical planar camera based on a wide-angle metasurface doublet corrected for monochromatic aberrations. *Nat. Comm.* 7 13682 (2016).

21. Khorasaninejad, M., Chen, W. T., Devlin, R. C., Oh, J., Zhu, A. Y., and Capasso, F. Metalenses at visible wavelengths: Diffraction-limited focusing and subwavelength resolution imaging. *Science*, 352(6290), 1190-1194, (2016).

22. Aieta, F., Genevet, P., Kats, M. A., Yu, N., Blanchard, R., Gaburro, Z. and Capasso, F. Aberration-Free Ultrathin Flat Lenses and Axicons at Telecom Wavelengths Based on Plasmonic Metasurfaces. *Nano lett.* 12, 4932 (2012).

23. Genevet, P., Yu, N., Aieta, F., Lin, J., Kats, M. A., Blanchard, R., Scully, M. O., Gaburro, Z., and Capasso, F. Ultra-thin plasmonic optical vortex plate based on phase discontinuities. *Appl. Phys. Lett.* 100 013101 (2012).

24. Aieta, F., Kats, M. A., Genevet, P. and Capasso, F. Multiwavelength achromatic metasurfaces by dispersive phase compensation. *Science* 347 6228, 1342-1345 (2015).

25. Arbabi, E., Arbabi, A., Kamali, S. M., Horie Y. and Faraon, A. Multiwavelength metasurfaces through spatial multiplexing. *Sci. Rep.* 6:32803 | DOI: 10.1038/srep32803.

26. Karimi, E., Schulz, S. A., De Leon, I., Qassim, H., Upham, J. and Boyd, R. W. Generating optical orbital angular momentum at visible wavelengths using a plasmonic metasurface. *Light: Science & Applications* 3 e167 (2014).

27. Jahani, S. and Jacob, Z. All-dielectric metamaterials. *Nat. Nanotechnol.* 11 23–36 (2016).

28. Yu, N., and Capasso, F. Flat optics with designer metasurfaces. *Nat. Mater.* 13 139–50 (2014).

29. Bao, Y., Jiang, Q., Kang, Y., Zhu, X. and Fang, Z. Enhanced performance of multifocal metalens with conic shapes. *Light: Science & Applications* 6, e17071 (2017).

30. Bao, Y., Zu, S., Liu, W., Zhou, L., Zhu, X. and Fang, Z. Revealing the spin-optics in conic-shaped metasurfaces. *Phys. Rev. B* 95, 081406(R) (2017).

## LIST OF SYMBOLS, ABBREVIATIONS, AND ACRONYMS

| | |
|---|---|
| AFRL | Air Force Research Laboratory |
| RXCC | Composites Branch, Structural Materials Division, Materials and Manufacturing Directorate |
| WPAFB | Wright-Patterson Air Force Base |
| MDL | Multi-level diffractive lens |
| MWIR | Mid-wave infrared |
| PSF | Point-spread function |
| MTF | Modulation-transfer function |
| FOV | Field of view |
| DOF | Depth of focus |
| FPA | Focal-plane array |
| LWIR | Long-wave infrared |
| POC | Proof-of-concept |
| FDTD | Finite-difference time-domain |
| DBS | Direct-binary search |
| NIR | Near-infrared |
| SWIR | Shortwave infrared |